PCCP

Accepted Manuscript

This is an *Accepted Manuscript*, which has been through the Royal Society of Chemistry peer review process and has been accepted for publication.

Accepted Manuscripts are published online shortly after acceptance, before technical editing, formatting and proof reading. Using this free service, authors can make their results available to the community, in citable form, before we publish the edited article. We will replace this *Accepted Manuscript* with the edited and formatted *Advance Article* as soon as it is available.

You can find more information about *Accepted Manuscripts* in the **Information for Authors**.

Imaging the C Black Formation by Acetylene Pyrolysis with Molecular Reactive Force Field Simulations

Chaoyang Zhang, *[†] Chi Zhang, [†‡] Yu Ma,[†] and Xianggui Xue[†]

[†] *Institute of Chemical Materials, China Academy of Engineering Physics (CAEP), P. O. Box 919-327, Mianyang, Sichuan 621900, China;*

[‡] *College of Chemistry and Chemical Engineering, Chongqing Universtiy, Chongqing 400044, China.*

Abstract C black is a class of substantial materials with a long history of applications. However, except from some descriptions on primary reactions, subsequent processes up to the final formation mechanism remain unclear. This mechanism is also crucial to understand the formation of other carbonaceous materials. In this work, we visualize C black formation by acetylene pyrolysis using molecular dynamic simulations with a molecular reactive force field named ReaxFF. We find that the formation undergoes four stages: 1) chain elongation by H abstraction and polymerization of small C species, 2) chain branching, 3) cyclization and ring densification, and 4) condensed ring folding. The simulated C black particle possesses a structure of folded graphite layers, in good accordance with experimental observations. Cyclization and condensation are derived from fusion among neighboring chains, significantly varying from common experimental observations at relatively low temperatures that abide by the mechanism of H abstraction and C_2H_2 addition. Moreover, polyyne and polyene are usually found in acetylene pyrolysis, suggesting that the pyrolysis of acetylene and other hydrocarbons may be a feasible method of obtaining carbyne, a novel carbonaceous material with high value.

Keywords C black, acetylene pyrolysis, formation mechanics, molecular dynamic simulation, ReaxFF, and carbyne.

1. Introduction

Carbonaceous materials such as fullerene, carbon nanotubes, and graphene, as well as composites based on these materials, have increasingly become research hotspots because of their excellent potential properties and performances [1–7]. However, these materials have not yet been applied extensively because of low yields. Controllable and efficient preparation is key to the applications of these materials.[8–10] On the other hand, the formation of C particles due to the incomplete combustion of carbonaceous fuels is one basic cause of air pollution. These C particles usually cause respiratory diseases and are therefore highly unwanted byproducts.[11] Increasing combustion completeness and decreasing the formation possibility of these particles require new technologies.[12] In addition, hydrocarbons such as acetylene provide a kind of H energy resource and pose an important issue of methods to increase H production and purity during H abstraction.[13,14]

Evidently, understanding the related mechanism for the controllable and efficient preparation of carbonaceous materials, the complete combustion of carbonaceous fuels, and H production is crucial. However, these processes usually occur under extreme conditions, such as high temperature, high pressure, electric discharge, and flame. In addition, these processes involve a series of complex homogeneous and heterogeneous reactions, causing difficulties in exploring the mechanism.[12] A recently developed reactive force field, ReaxFF, provides an opportunity to overcome these difficulties. The use of ReaxFF can be feasible in large-scale systems involving numerous reactions. In addition, this technology has been successfully applied to heated and shock explosives, fuel combustion, and pyrolysis, with the aid of chemical quantum and kinetic calculations[15–24]. In systems involving several hundred millions of atoms, the ReaxFF molecular dynamic (MD) method can offer results comparable to *ab initio* MD simulations or experiments.

An understanding of mechanisms involved in the formation of above-mentioned carbonaceous

materials and particles, as well as H production, can be exemplified by the mechanism of C black formation by acetylene pyrolysis. Acetylene was selected because the organic compound is a common source and precursor of the C materials. In addition, acetylene pyrolysis has been the object of several studies, which provide basis for this work. This work intends to visualize acetylene pyrolysis by the molecular reactive force field, ReaxFF.

C black is a class of important materials that is extensively applied to improve structural, mechanical, electric, optical, and catalytic properties.[25–28] This material is produced by the incomplete combustion or decomposition of carbonaceous substances and possesses a history of use spanning about two centuries. C black is a light, soft, and amorphous C form with extremely high specific surfaces and common sizes of 5 to 50 nm. Microscopically, both graphite-like crystal structures and amorphous structures are believed to be involved in C black. Earlier X-ray diffraction analyses showed that C black particles are composed of microcrystalline structures with several folding layers. The layer structures are graphitic, with greater interlayer distances of 0.34 to 0.41 nm relative to graphite. Meanwhile, stacking of distorted and inserted layers leads to amorphous structures in C black particles. Subsequently, transmission electron microscopy and high resolution phase-contrast microscopy examinations confirmed the ordered stacking of microcrystalline structures, instead of the random stacking suggested by X-ray diffraction analyses results. Local crystal structures and wrinkled steps were recently found using scanning tunnel microscopy and atomic force microscopy methods.[29–32]

Two pathways are believed to be involved in the formation mechanism of C black by acetylene pyrolysis. These pathways are molecular and radical additions, which are favored at low and high temperatures, respectively. The H abstraction and C_2H_2 addition (HACA) mechanism[33] for polycyclic aromatic hydrocarbons (PAHs) and final C black nucleation and formation is widely

accepted. Several pioneering works showed that acetylene pyrolysis consists of the first important reaction step toward the initial formation of vinylacetylene (C_4H_4) and diacetylene or 1,3-butadiyne (C_4H_2).[34–37] Successive reactions form PAHs and C black precursors. The increase in PAH sizes and final C black formation can be explained by the so-called HACA mechanism. In fact, data on observed chemical species during acetylene pyrolysis are still limited. For example, molecules range from H_2, methane, and benzene[38], to heavy PAHs, such as dibenzo(a,h)anthracene ($C_{22}H_{14}$), benzo(g,h,i) perylene ($C_{22}H_{12}$), and coronene ($C_{24}H_{12}$) [39-44]. Radicals include C_4H_4, C_4H_2, C_6H_2 (1,3,5-hexatriyne), and C_8H_2 (1,3,5,7-octatetrayne) [45,46]. Structures and components of multiple depositions in pyrolysis have not been confirmed, and numerous intermediates and products have only been kinetically deduced. Therefore, we can conclude that C black formation processes remain unclear, which is attributed to the high complexity of the processes. In particular, the growth mechanism of C black particles cannot be fully explained by the HACA theory.

Full-atom simulations can image the entire evolution of these complex reactions and provide opportunities to explore the formation mechanism. By ReaxFF MD simulations, we reveal four stages of C black formation by acetylene pyrolysis. In addition, we discover numerous C chains, including polyyne and polyene, during the formation. Moreover, isolated benzene molecules were not found in our simulations. This finding significantly varies from previous observations and conjectures, possibly leading to a deeper insight into the pyrolysis at higher temperatures. Furthermore, by employing the same methods applied here, we believe that the pyrolysis of other hydrocarbons can be imaged.

2. Simulation Methodologies

Simulating acetylene pyrolysis requires adequate structures and conditions. In our simulations, 1000 C_2H_2 molecules were contained in two cubic cells with lengths of 75.61 and 137.4 Å, which

correspond to densities of 0.1 and 0.01 g/cm^3, respectively. In contrast to the density at standard state of 0.0017 g/cm^3, these C_2H_2 in cells were greatly compressed to a density enhanced about 60 times. This compression, which leads to a higher pressure and a higher concentration of C_2H_2, will increase reaction velocities and shorten the time to attain equilibrium at the same temperature in terms of chemical kinetic theory. That is, within the time limitation of our simulations, more information will be obtained for the compressed C_2H_2. Acetylene black is usually formed by the incomplete combustion of acetylene, which has a flame temperature exceeding 3000 K. Therefore, three temperatures 2500, 3000, and 3500 K were assigned for simulations. Moreover, it should be noted that industrial flame processes for manufacturing C-black may operate at pressures of just a few atm or so with C-black accumulating in pre-flame regions with temperatures hovering around 2000-2500 K, i.e., there is much enhancement of temperatures and pressures applied for simulations. While, this enhancement suggest an implication, e.g., one would expect recombinations to be more active at these enhanced temperatures and pressures, even though the mechanism of C-black growth may not exactly operate under such simulation conditions.

(a)   (b)
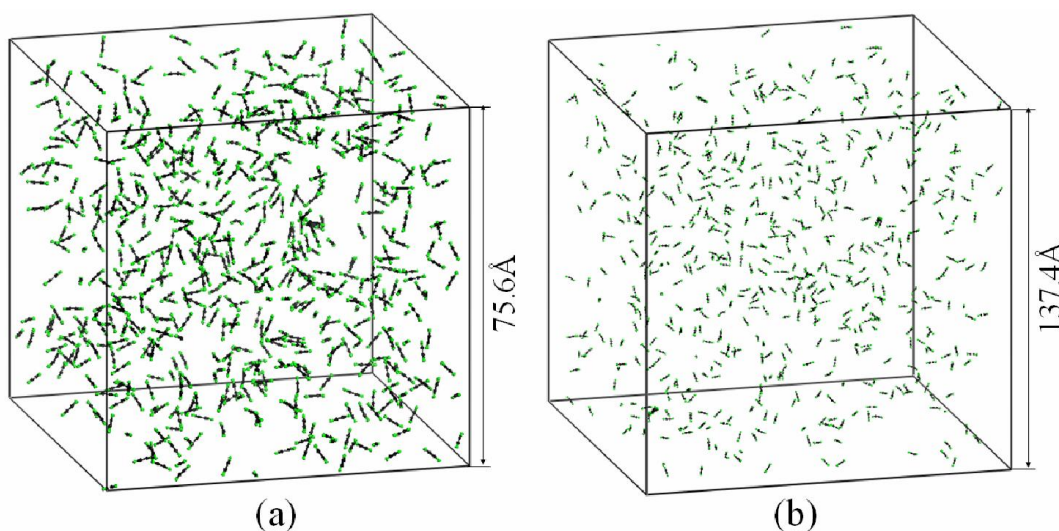
Fig. 1 Cubic cells containing 1000 C_2H_2 molecules for modeling. (a) d = 0.1 g/cm^3 and (b) d = 0.01 g/cm^3. C and H atoms are represented in black and green, respectively. This representation is considered in the following figures.

Canonical particle number (N), volume (V), and temperature (T) conditions (NVT), and the

above-mentioned molecular reactive force field ReaxFF combined with MD method in a LAMMPS package[47,48] were employed to simulate the related evolution resembling acetylene pyrolysis. A total of six simulations were performed. Fig. 1 shows the two cells, each covering two densities and three temperatures. Simple Nosé–Hoover thermostat method [49] was adopted in these simulations, and the time-step and effective relaxation time were assigned as 0.1 and 20 fs, respectively. Specifically, the coupling frequency of the thermostat to nuclear motion was composed of 200 time-steps. Each cell was relaxed using an NVT MD simulation at 300 K for 10 ps, and no C_2H_2 decay was found prior to heating to the assigned temperatures. Then, six independent simulations were performed for 5 ns, and the atomic positions and velocities were recorded every 1 ps, namely, 5000 frames were used for trajectory analyses.

The principle of ReaxFF method can be found in the literature[50]. In a typical procedure, ReaxFF is an improved force field derived from earlier reactive empirical force fields, such as those by Brenner, which are parameterized to reproduce the density functional theory (DFT) results for selected systems and properties[51,52]. ReaxFF is a reactive force field based on the bond-order principle. That is, the bond orders are updated each MD step, thus allowing the ReaxFF to recognize new bonds and to break existing bonds between the atoms of reacting molecules. The instantaneous valence force and interaction energy between two atoms is determined by the instantaneous bond order, which in turn is determined by the instantaneous bond distance. At the same time, other valence interactions are written in terms of the bond order so that they all go smoothly to zero as bonds dissociate. Also, the instantaneous bond orders are subsequently corrected with overcoordination and undercoordination terms designed to favor formation of the proper number of bonds. Thereby, the bond energy is a function of bond length (E_{bond}), valence angle (E_{val}), torsion angle (E_{tor}), lone pair (E_{lp}), conjugation (E_{conj}), overcoordination (E_{over}), undercoordination (E_{under}) and penalty (E_{pen}). Besides, a two-body van der Waals (E_{vdW}) is included to ensure a proper description of the short-range repulsion due to the Pauli principle and the long-range van der Waals attraction (London dispersion). In ReaxFF, the instantaneous charge on

each atom is determined by the electrostatic field due to all other charges in the system plus a simple, second-order description of the dependence of the internal energy of the atom on charge (expressed in terms of electronegativity and hardness). The interaction ($E_{Coulomb}$) between two charges is written as a shielded Coulomb potential so that it is well-behaved, even between bonded atoms. Overall, the total energy of a system in ReaxFF is described as eq (1)[50]

$$E_{system} = E_{bond} + E_{lp} + E_{over} + E_{under} + E_{val} + E_{pen} + E_{tors} + E_{conj} + E_{vdW} + E_{Coulomb} \qquad (1)$$

In this work, three kinds of atomic pairs of C-C, C-H and H-H are present, whose bond order cut-offs are assigned to 0.55, 0.4 and 0.55 as usual, respectively. ReaxFF has been successfully applied in studying the reactions of hydrocarbons with a wide temperature range of 773.15-3500 K [21,22,53-58], suggesting its reliability in the present study dealing with acetylene pyrolyses at 2500, 3000 and 3500 K. Besides, a post-processing program for ReaxFF simulation of chemical structural model of coal was currently developed to understand its thermal reaction mechanisms, verifying the reliability of the force field to carbonaceous systems[59].

3. Results and Discussion

As mentioned above, ReaxFF MD simulations were performed separately on two acetylene cells with densities of 0.01 and 0.1 g/cm^3 and temperatures of 2500, 3000 and 3500 K. After careful examination, we find that acetylene pyrolysis in the cell with a density of 0.1 g/cm^3 at 3500 K proceeds the fastest, which is as expected, because of the highest concentration and temperature. In this case, pyrolysis is nearly finished after about 2 ns, so analyses and discussion within this time range are adequate, whereas, for other cases, reactions do not reach completion within the simulation time limit of 5 ns. Moreover, by comparing snapshots in Figs s1, s2, and s3 of Electronic Supplementary Information (ESI) with those in Fig. 2, we find that the six simulations exhibit a similar evolution mechanism, only varying in evolution velocities. That is, to more comprehensively understand C black formation mechanism, we mainly discuss the simulation

results in the case of 0.1 g/cm^3 and 3500 K as follows, unless otherwise specified.
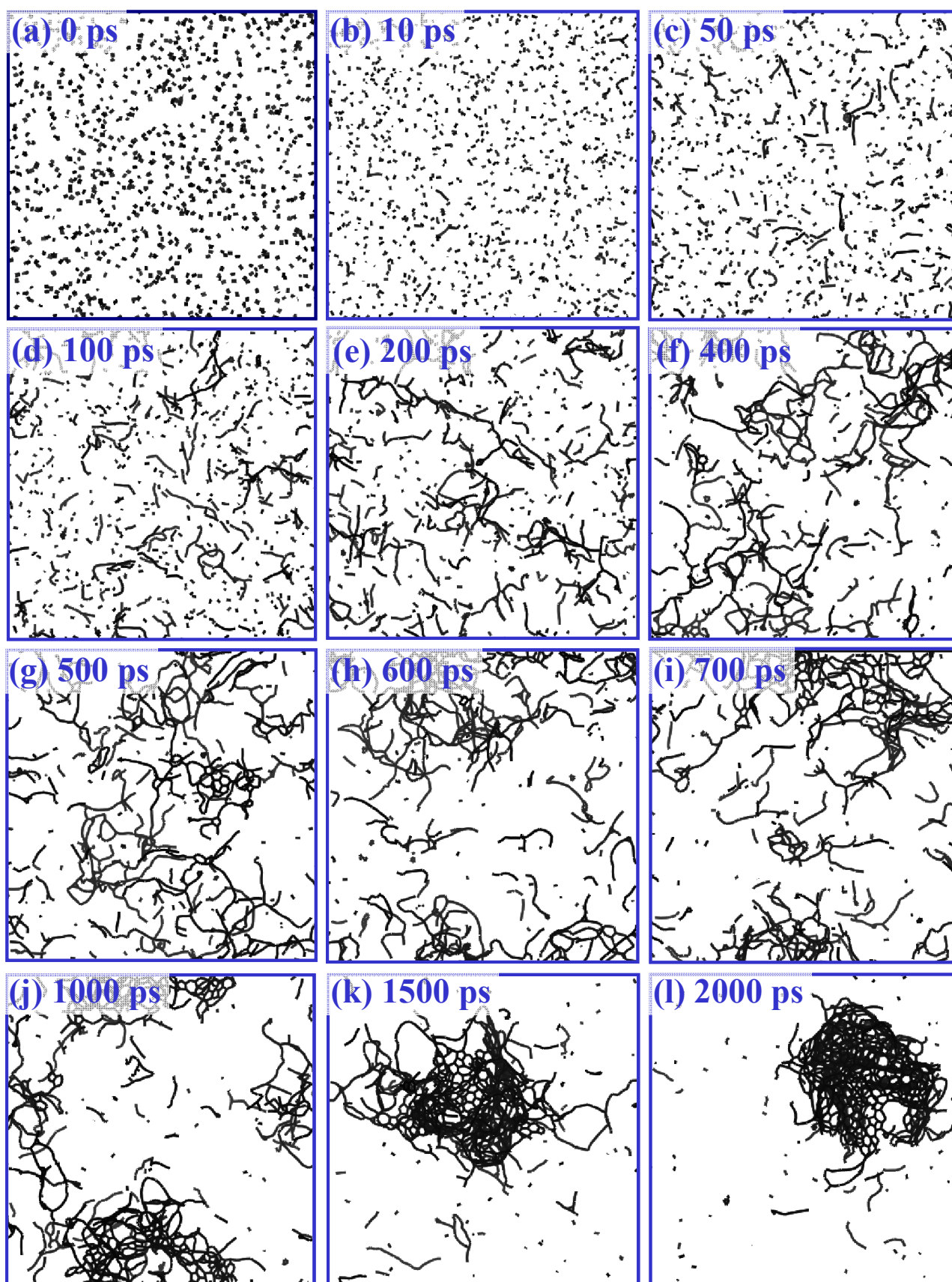
Fig. 2 Snapshots of acetylene pyrolysis with time. Only carbon atoms are exhibited for clarity. (a) to (l) correspond to 0, 10, 50, 100, 200, 400, 500, 600, 700, 1000, 1500, and 2000 ps, respectively.

3.1 Chemical Species and Their Evolution
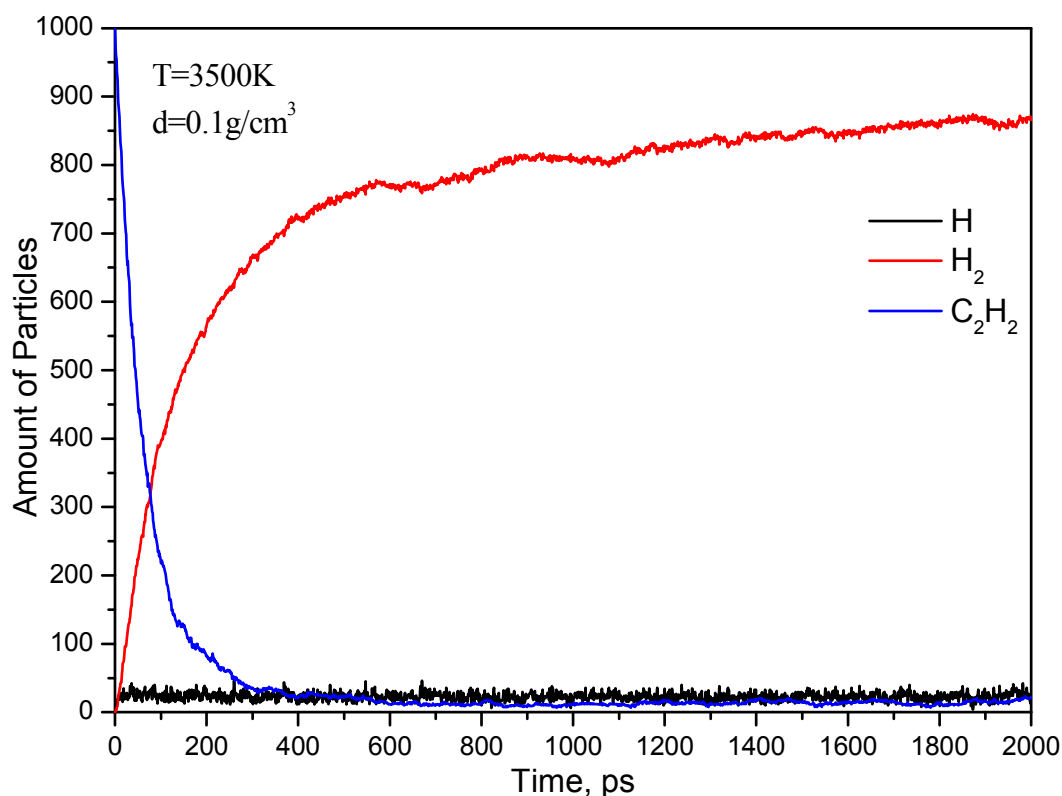
Fig. 3 Evolution of C_2H_2, H_2, and H.

$$C_2H_2 \rightarrow C \text{ (graphite)} + H_2 \quad (2)$$

The conversion of C_2H_2 into perfect graphite and H_2 (reaction 2, which is an overall reaction) is thermodynamically favored because of the released 226.7 kJ/mol heat in the standard state[60]. Reaction 2 cannot be realized at a conventional temperature, whereas heating can make the reaction feasible. Heating C_2H_2 produces numerous radicals and molecules, including atomic H, H_2, and various C species, through numerous reactions. As time elapses, H atoms are first abstracted from C_2H_2, and some of these atoms are combined pair-wise to form H_2. As demonstrated in Fig. 3, both the decay of the reactant C_2H_2 and the increase in H_2 rapidly proceed within the initial 300 ps. Thereafter, these changes evolved slowly as the number of C_2H_2 molecules decreases to 20 and fluctuates around this value after 600 ps, and as H_2 increases gradually to 870 at a time of 2000 ps. For atomic H, only several picoseconds are required to reach a dynamic equilibrium amount of 25 afterwards.
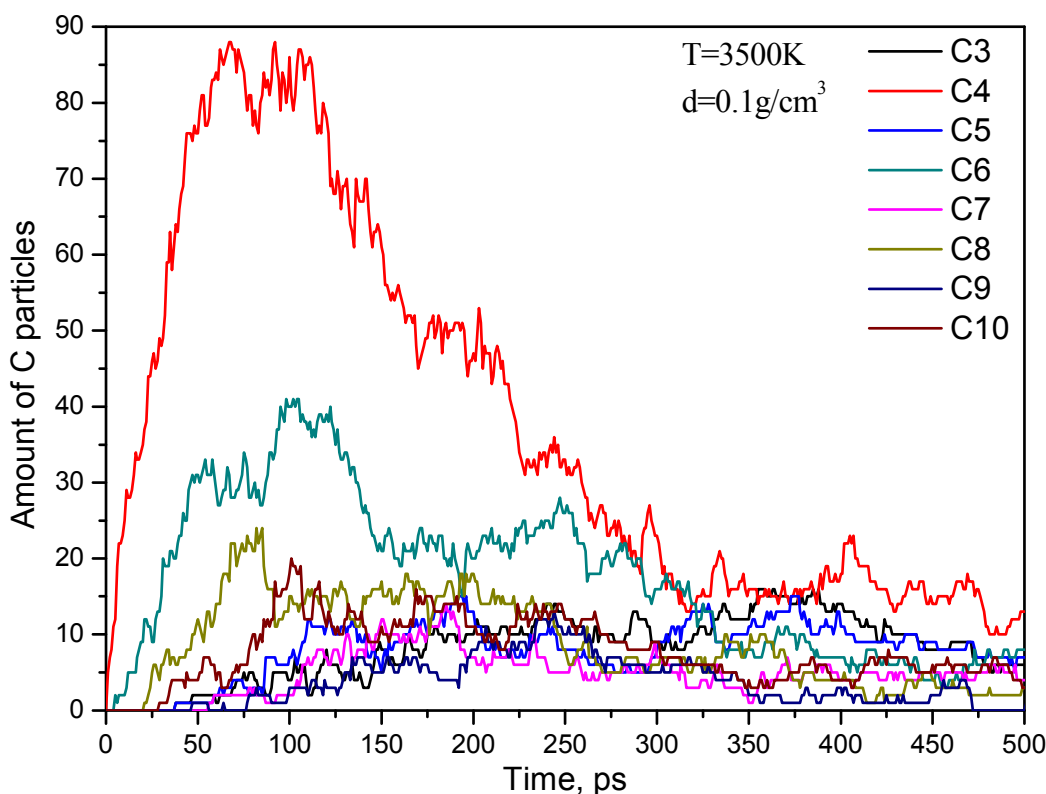
Fig. 4 Evolution of C3 to C10 species within the initial 500 ps.

Regarding C species resulting from the C_2H_2 decay at 3500 K, the species possess a numerous kinds with varying amounts, and most of these species are composed of single to multiple radicals. For convenience, we distinguish these species in terms of the numbers of C atoms they contained (*n*), regardless of the numbers of H atoms attached on them, and call them C*n*. At an earlier stage, the oligomerization of C_2H_2 occurs with small dissociations. As illustrated in Fig. 4, at an *n* range of 3 to 10, the amounts of C*n* with even *n* (i.e., C4, C6, C8, and C10) notably reached larger maxima than those with odd *n* (i.e., C3, C5, C7, and C9). In addition, lower even *n* corresponds to larger maxima, while C*n* with higher even *n* are generated later. A similar conclusion can be drawn for other Cn with *n* ranging from 11 to 20, as shown in Fig. s4 of ESI. In combination with the decrease in C_2H_2, these results suggest acetylene polymerization by consuming low C species.
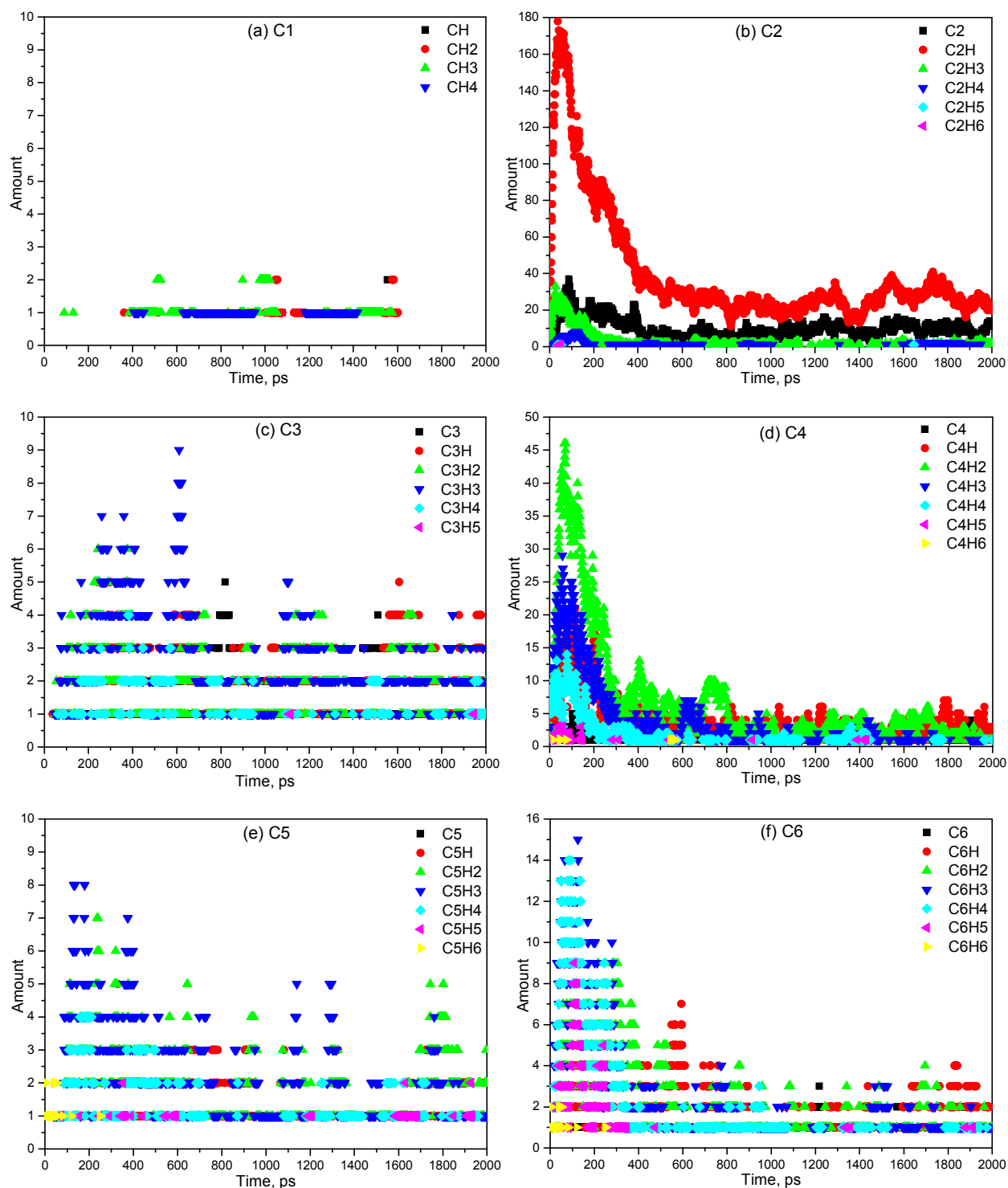
Fig. 5 Evolution of the amounts of various C species at T=3500 K and d=0.1 g/cm^3. (a) C1, (b) C2, (c) C3, (d) C4, (e) C5, and (f) C6.

Considering that primary structures and related amounts are crucial to the formation of the final C black, we carefully checked all Cn (n = 1 to 6) during the initial 2000 ps. For C1, no isolated C atom is found. In addition, C1 exists in four types, namely, CH, CH$_2$, CH$_3$, and CH$_4$, all with small amounts, that is, only one or two C1 are found in Fig. 5(a). In contrast to other C species, C1

species are formed at a later part of the process. CH, CH_2, CH_3, and CH_4 appear at 1078, 361, 90, and 407 ps, respectively, whereas C1 seldom exists. C2 is immediately produced after C_2H_2 molecules were heated to 3500 K. C_2, C_2H, C_2H_3, C_2H_4, C_2H_5, and C_2H_6 appear after 1, 1, 1, 2, 36, and 41 ps, respectively. Remarkably, as demonstrated in Fig. 5(b), C_2, C_2H, and C_2H_3 are found in higher quantities than other newly formed species. This finding from the simulation suggests that the primary reactions in the acetylene pyrolysis include $C_2H_2 \rightarrow C_2H + H$, $C_2H \rightarrow C_2 + H$ and $C_2H_2 + H \rightarrow C_2H_3$. C_2H_4, C_2H_5, and C_2H_6 are considered as products of H addition, and their amounts can be as insignificant as those of C1, thus implying that these addition reactions can be negligible, as well. This result coincides with previous experimental observations at relatively low temperatures[34–37,45,46]. For C4 species, Fig. 5(d) shows the predominant populations of C_4H_2 and C_4H_3, which are formed by the following addition reactions of C_2H with C_2H and C_2H_2: $C_2H + C_2H \rightarrow C_4H_2$ and $C_2H + C_2H_2 \rightarrow C_4H_3$. C_4H_4, C_4H_5, and C_4H_6 are also produced in C2 addition, but with lower populations. The population differences of these C4 species are dominated by the concentrations and addition activities of C2. As illustrated in Fig. 5(b), the active C_2H is greater than other C2 species, resulting in the dominant population of C_4H_2 species through the reaction of $C_2H + C_2H \rightarrow C_4H_2$. At the same time, the higher population of C_4H_3 is attributed to the excessively high concentration of the primary reactant C_2H_2, even though C_2H_2 does not possess the highest addition activity among all C2 species. Regarding C6, C_6H_3 and C_6H_4 present the highest populations (in Fig. 4(f)) during the evolution of heated C_2H_2. We can rationally deduce that these two species were derived from the additions of $C_2H + C_4H_2$ and $C_2H + C_4H_3$, respectively, because of their higher concentrations and reactivity. These simulated results agree with previous observations and conjectures [45,46]. Significantly varying from observations at low temperatures, stable benzene ring structures were not found[38] in simulations at a high temperature of 3500 K.

Careful examination shows C_6H_6 presents a linear structure, instead of one composed of six-membered rings.

With respect to C3 in Fig. 5(c) and C5 in Fig. 5(e), the species were generated later in the reaction, like C1. We think that this later formation translates to the dissociation of addition (polymerization) products. The direct dissociation of C_2H_2 to CH occurs a greater difficulty than to C_2H and H, because HC≡CH bond is considerably stronger than $H-C_2H$ bond, with bond dissociation energy of 954 kJ/mol in contrast to 557.8 kJ/mol[60]. That is, the C species with odd C atoms are formed with an advanced polymerization prerequisite. Moreover, extremely small quantities of these species show that polymerization is predominant in the primary stage.

From the above discussion on the initial stage of C chain elongation, we can conclude that the formation of short C chains obey the HACA mechanism[33]. However, no six-membered ring has been found in the simulations.

As time proceeds, polymerization increases the sizes of certain C species, decreases the total amounts of low C species, and leads to the final formation of C black particles. Other species like C11 to C20 have been determined and found, as shown in Fig. s4 of ESI. In addition, tens of molecules with more than 20 C atoms, which are polymerization or dissociation products, have also been examined out through trajectory analyses. These molecules possess a polymerization base of C_2H, which is one of the first products of acetylene pyrolysis. The evolution of large C particles will be discussed in the next section.

3.2 Formation Mechanism of Carbon Black

We trapped several typical snapshots in Fig. 2 to represent different stages of C black formation. As demonstrated in the figure, formation can be divided into the following stages.

(1) Chain elongation. Fig. 2(a) exhibits the primary state of C_2H_2. All C_2H_2 molecules are

evenly and randomly dispersed as a solute dissolved in solution. In Fig. 2(b), several elongated chains are found. However, the chains found at this time are relatively short this time, with 6 C atoms found on the longest chains. As time reached 50 ps, the C atoms on the longest chains increase to 50, as shown in Fig. 2(c). Unlike acetylene pyrolysis at relatively low temperatures, pyrolysis at 3500 K can cause the formation of straight chains, each with tens of C atoms, instead of cyclization once the amount of C atoms reaches six. Upon carefully examining these straight chains, we find significantly few H atoms linked. That is, one-dimensional straight chains should be ascribed to polyyne and polyene. The formation of polyyne and polyene should be attributed to the end–end additions of short chains. Explicably, end–end additions are more active than end–midst or the midst–midst ones. Meanwhile, the lack of benzene formation may be due to the high rigidity of C6 chains, which causes considerably less opportunity for intramolecular cyclization than intermolecular chain elongation.

(2) Chain branching. As time resumes, chain length increases, and branched chains appear, as exhibited in Figs 2(d) and 2(e). These branched chains are the results of the end–midst fusion of neighboring straight chains. Although the ends of chains are more active than the midst sites, the midst sites are more kinetically dominant during addition than the ends, because of their substantially higher concentration. That is, chain branching is a necessary result when the chains reach a certain extent.

(3) Cyclization and cycle condensation. Cyclization of these branched chains subsequently occurs. Cyclization resulted from the fusion of neighboring C chains, instead of the curvature of isolated straight chains, which cannot be explained by the HACA mechanism [33]. Similar to above branching caused by multiple active sites on midst and terminals of C chains at high temperatures, cyclization is induced by these active sites, as well. As indicated on the bottom-left section of Fig.

2(f), an evident five-membered ring was found. In fact, five- to eight-membered rings are observed, agreeing with a recent quantum chemical molecular simulation results on C deposition, in which these rings appear[61]. Thermodynamically, cyclization, particularly to six-membered rings, aids in decreasing energy and stabilizing the system. Therefore, further cycle condensation is reasonable as nucleation occurs in C black formation. Condensed rings can be seen in Fig.s 2(g) (middle), 2(h) (top), and 2(i) (top and bottom).

(4) Folding of condensed rings and final formation of C black. As demonstrated in Fig. 2(j), at 1000 ps, C_2H_2 evolves into an amorphous system composed of H_2, straight and branched C chains, and fused C cycles. As time elapses, most straight and branched C chains are converted into C cycles, and then folding begins after the densification of these cycles (Fig. 2(k)). The folded, fused cycles consist of the final C black (Fig. 2(l)), which is in agreement with experimental observations [29–32].
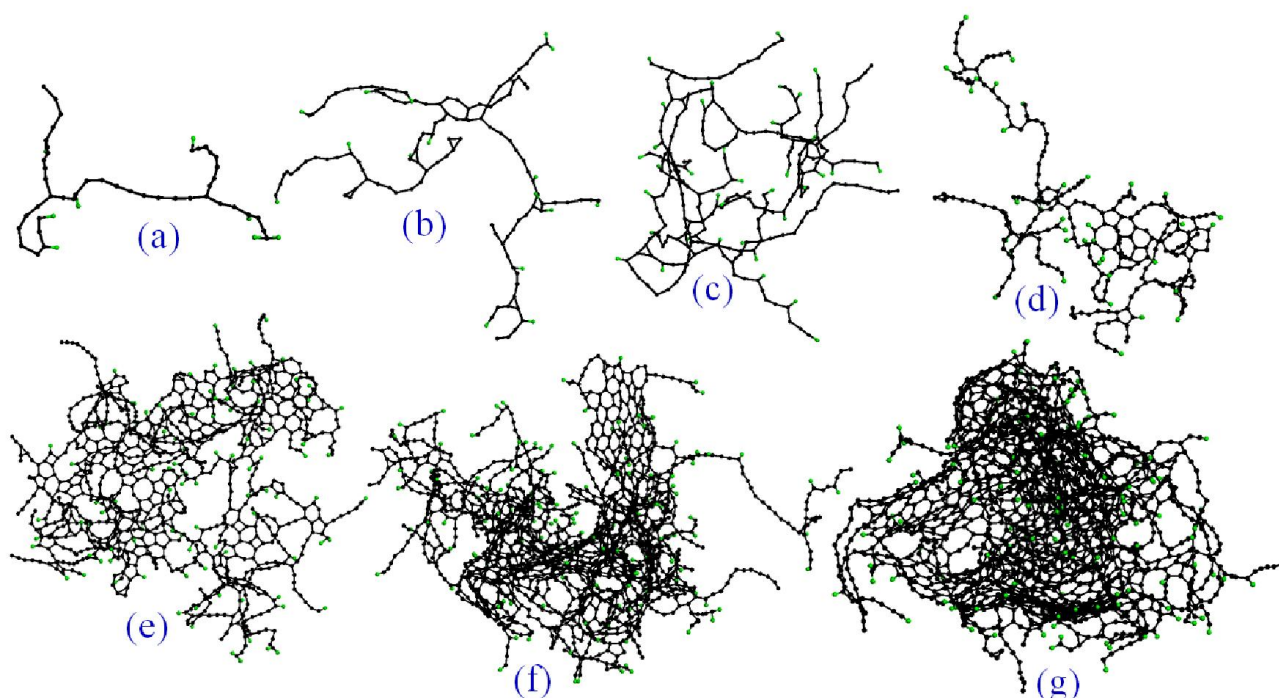

Fig. 6 Typical structures showing the stages in C black formation. (a) chain branching, (b) cyclization, (c) more branching and more cyclization, (d) ring condensation, (e) folding, (f) more condensation and more folding, and (g) final formation of C black.

In total, the typical snapshots in Fig. 2 can show the formation mechanism of C black, a large

C particle. To show typical structures representing different stages more clearly, we abstracted some of these structures in Fig. 6. From the figure, we can readily distinguish the structures mentioned above, namely, branched chains, rings, condensed rings, and folded condensed rings. In particular, several polyyne and polyene chains are found to be chemically bonded in or with these structures. These findings imply that carbyne[62–64] can be prepared through acetylene pyrolysis if we can control the condition perfectly by preventing branching and cyclization, because of a stability prediction at high temperatures[62].
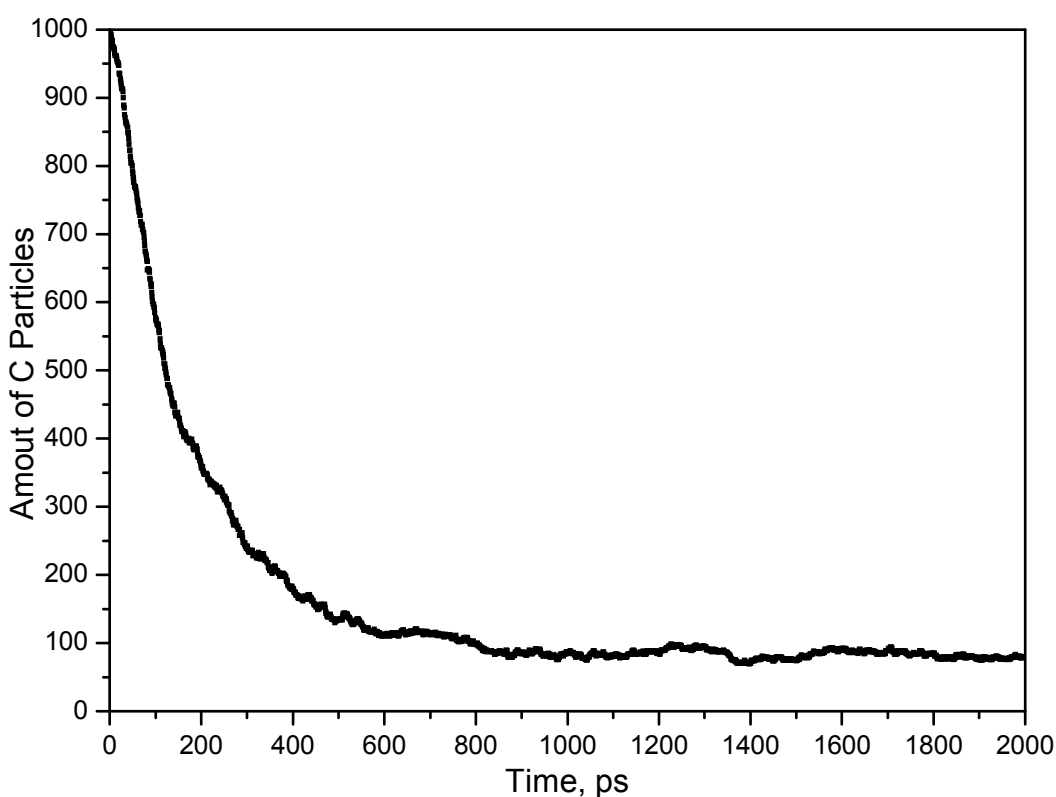
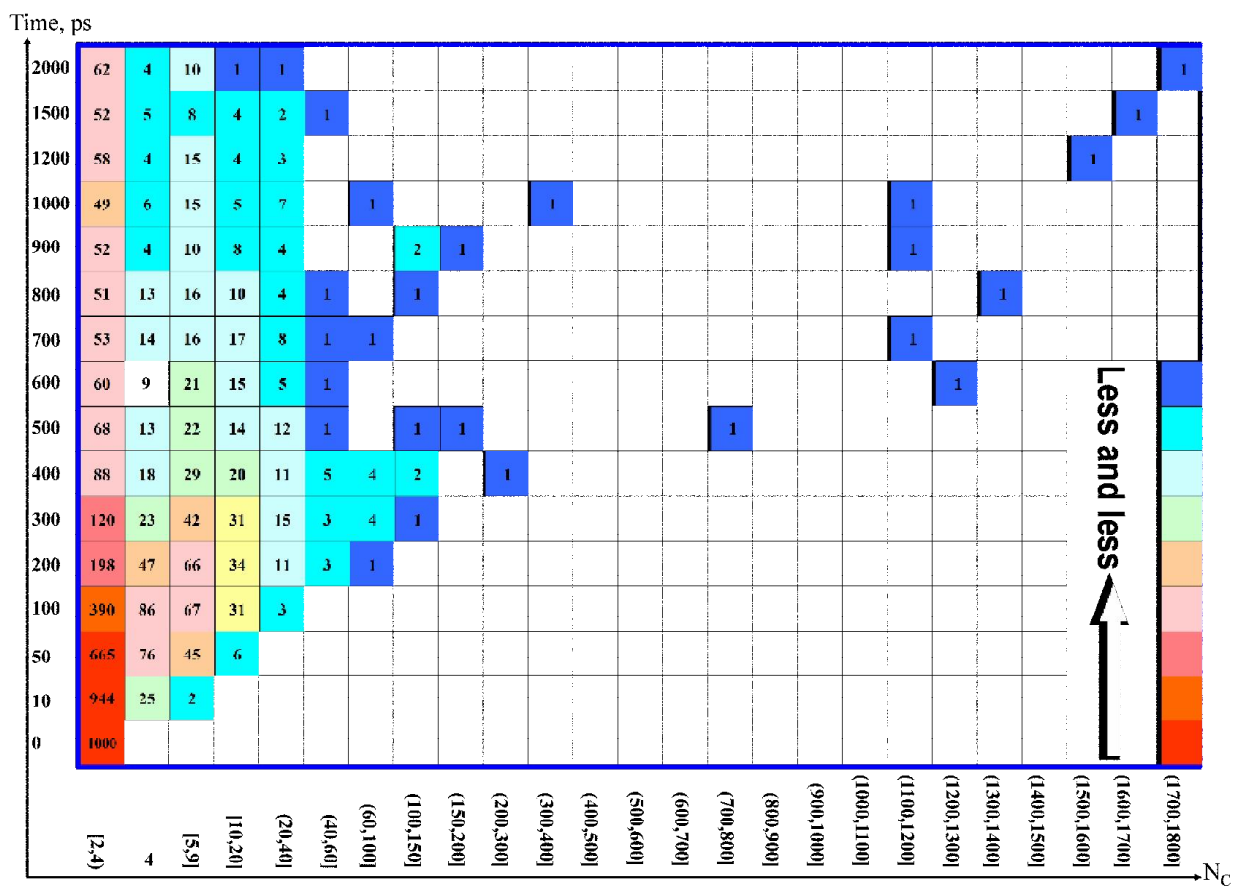**Fig 7** Evolution of the total amount of C species.

Fig. 8 Evolution of C species. N_C is the number of C atoms in the species.

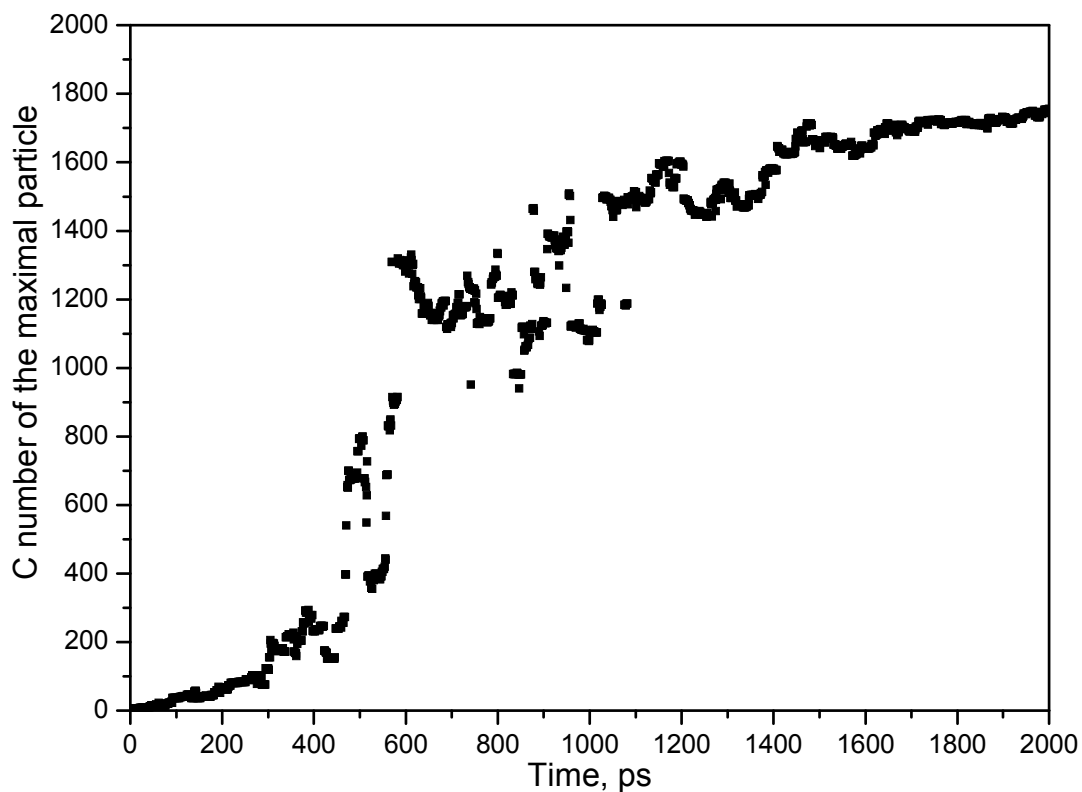| Time, ps	[2,4]	4	[5,9]	[10,20]	(20,40]	(40,60]	(60,100]	(100,150]	(150,200]	(200,300]	(300,400]	(400,500]	(500,600]	(600,700]	(700,800]	(800,900]	(900,1000]	(1000,1100]	(1100,1200]	(1200,1300]	(1300,1400]	(1400,1500]	(1500,1600]	(1600,1700]	(1700,1800]
2000	62	4	10	1	1																				1
1500	52	5	8	4	2	1																		1	
1200	58	4	15	4	3																		1		
1000	49	6	15	5	7	1				1									1						
900	52	4	10	8	4			2	1										1						
800	51	13	16	10	4	1		1													1				
700	53	14	16	17	8	1	1												1						
600	60	9	21	15	5	1														1					1
500	68	13	22	14	12	1		1	1						1										
400	88	18	29	20	11	5	4	2		1															
300	120	23	42	31	15	3	4	1																	
200	198	47	66	34	11	3	1																		
100	390	86	67	31	3																				
50	665	76	45	6																					
10	944	25	2																						
0	1000																								

Fig. 9 Evolution of the C number of the maximal C species.

As is evident, the final formation of C black with a large quantity of C atoms consumes

numerous small C species. Fig. 7 exhibits the evolution of the total amount of all C species: a sharp

decrease until 600 ps, followed by a gradual decrease thereafter to a final equilibrium amount of

about 70. To describe the evolution of C species in more detail, we are required to investigate their

distributions against time. From Fig. 8, we can readily conclude that C species are evolved from the

initial small sizes and large quantities to final large sizes and small quantities. During particle

growth and besides the above-mentioned polymerization, fusion among big particles also performs

an important function. For example, fusion causes an explosive increase in the C number of the

maximal C species, which presents a content of the most C atoms among all chemical species,

during a period of 300 to 600 ps, as demonstrated in Fig. 9. Typically, as is shown in Fig. 8, when

time proceeds from 500 ps to 600 ps or from 1000 to 1200 ps, the formation of larger particles

consumes large species. From 500 ps to 600 ps, one C (1200, 1300] particle is formed at the cost of

one C (100,150], one C (150,200], and one C (700,800] particles. Similarly, at 1000 ps to 1200 ps,

the formation of one C(1500, 1600] particle consumes one C(60,100], one C(300,400], and one

C(1100,1200] particles. Understandably, the explosive growth does not occur by means of

step-by-step additions of C_2H, which is the first pyrolysis product of C_2H_2.

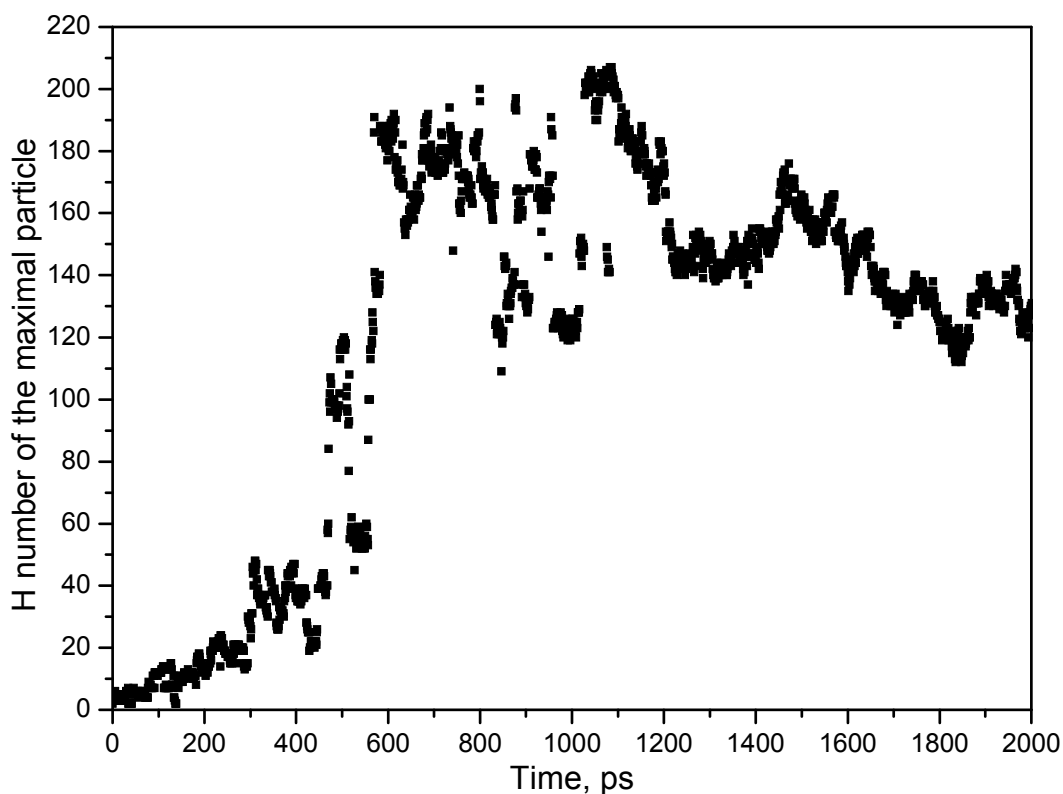**Fig. 10** Evolution of the H number of the maximal C species.
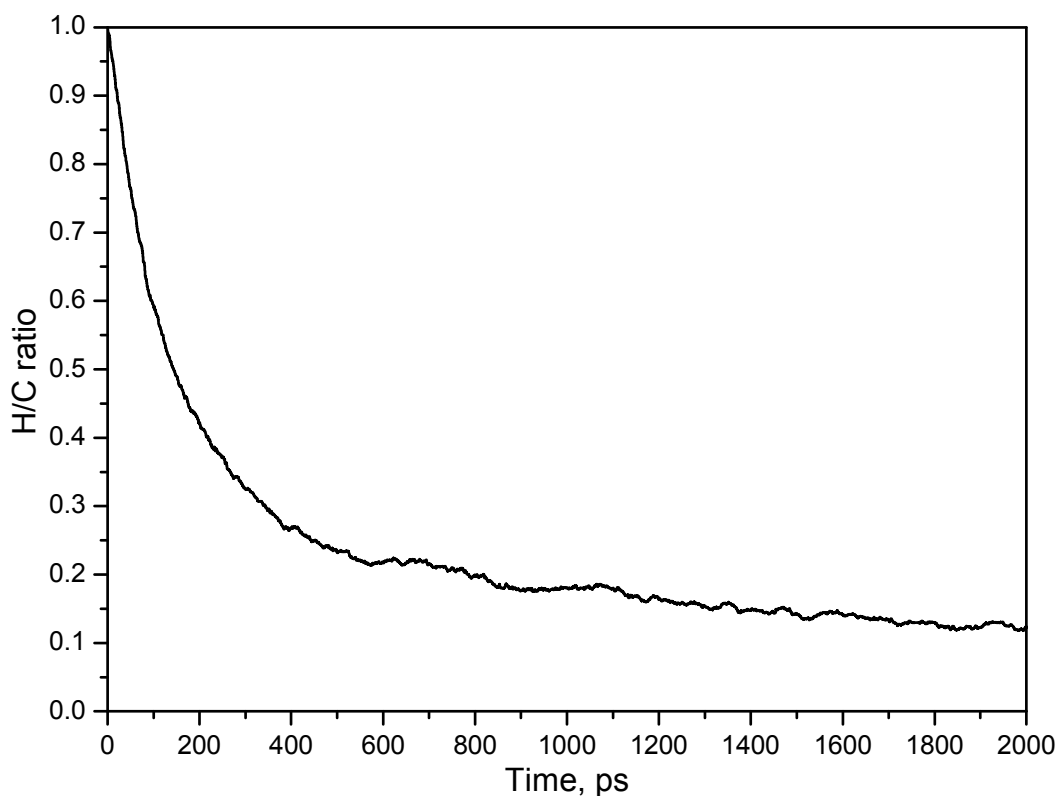

Fig. 11. Evolution of the H/C ratios of the maximal particles.

On the other hand, H abstraction proceeds continuously during the formation of the maximal

species. Fig. 10 exhibits a first increase, a subsequent fluctuation, and a final decrease of H atoms in

the maximal species, which are reasonable. By both addition and fusion, the formation of larger

species will initially increase H atoms. Then, fluctuation is generated by formation–dissociation–formation of the large particles. This progression can be deduced from Fig. 9, which exhibits a fluctuation of C numbers, as well. The final decrease is caused by continuous H abstraction from the stable maximal C species. In other words, H atoms are continuously dissociated from C species to form C black within the simulation time range, leading to a successive decrease in H/C rates in Fig. 11, which is in agreement with the increase in abstracted H atoms (including atomic and molecular) in Fig. 2.
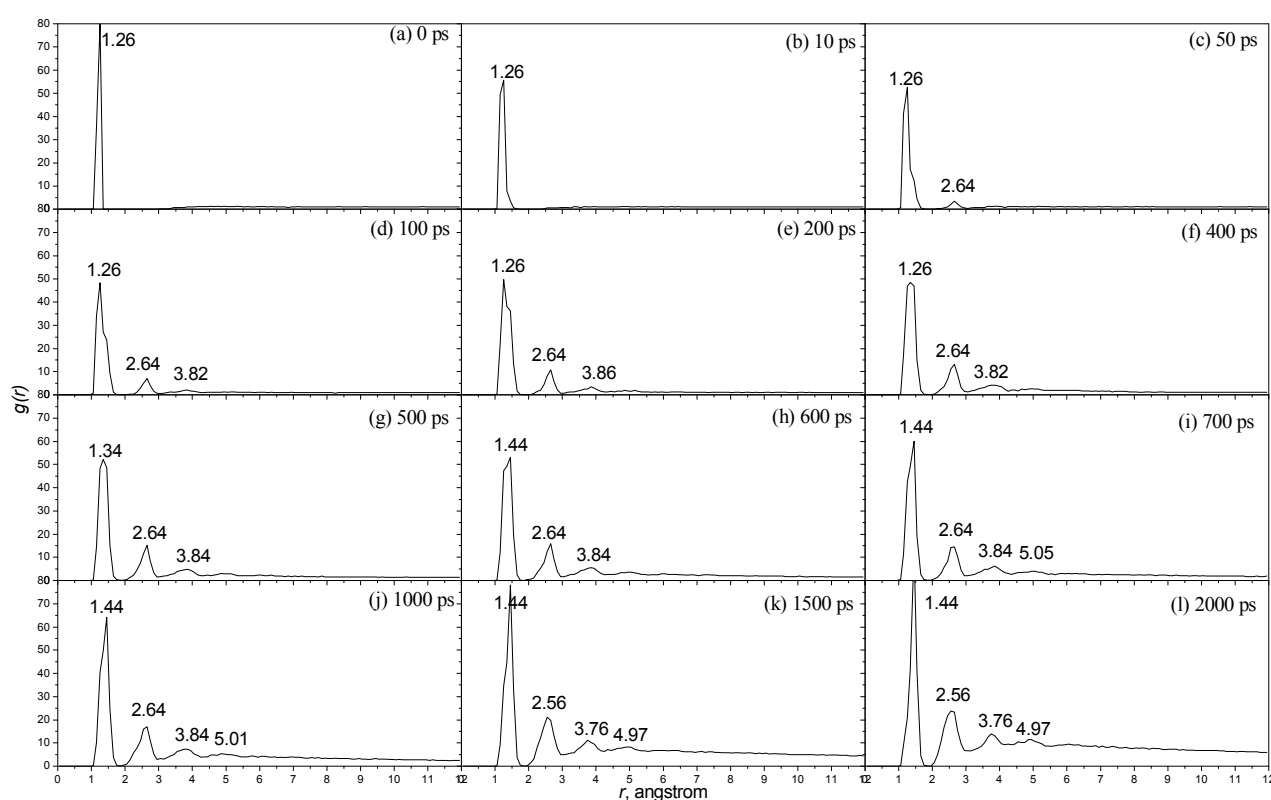
Fig. 12 Radial distribution functions (RDFs) of C-C at different times.(a) to (l) correspond to 0, 10, 50, 100, 200, 400, 500, 600, 700, 1000, 1500, and 2000 ps, respectively.

Furthermore, the chemical bonds between C atoms are involved, because bond types reflect the related structures. For this complex system, a statistical method of radial distribution function (RDF, g(r)), which provides the distances of assigned atomic pairs within a cutoff,[65] was employed for analysis. Corresponding to Fig. 2, we obtain C-C RDFs from Fig. 12. Within 0 ps to 400 ps (Figs 12(a) to 12(f)), the dominant C-C distances are 1.26 Å as a found g(r) peak, which is slightly longer than that in alkyne because of the high temperature of 3500 K (e.g., 1.186 Å for acetylene at 131

20

K[66]). This finding suggests that the orders of C-C bonds are mainly triple in this period. As time

proceeds, the g(r) of 1.26 Å is gradually eroded, and the predominant g(r) changes to a site of 1.34

Å (Fig. 12(g)), implying that most C-C bonds are elongated to double C-C bonds (e.g., 1.314 Å for

ethylene at 131 K[67]). These findings should be ascribed to the addition reactions, which are in

accordance with the chains observed in Fig. 2(g). At a time of 600 ps (Fig. 12(h)), g(r) is mainly

located at 1.44 Å, which is slightly longer than the C-C bond length of graphite at room temperature

(the slight elongation resulted from high temperature, as well). In addition, the g(r) at this site

becomes increasingly acute thereafter (Figs 12(h) to 12(l)), suggesting a higher degree of perfect

cycle condensation.
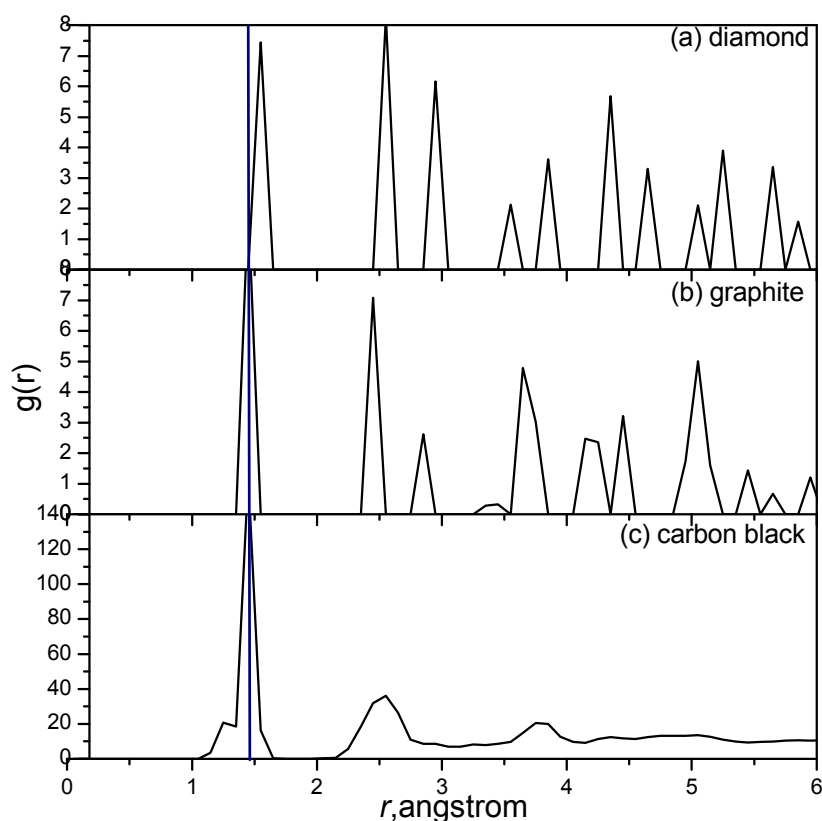
Fig. 13 C-C RDF comparison of diamond (a), graphite (b), and simulated C black (c).

To further confirm the bonding type of the final maximal C particle, we examined its RDFs

and compared them with those of diamond and graphite. As illustrated in Fig. 13, simulated C black

and graphite possess similar main RDFs, implying similar structures. However, a difference exists

between them, given by other acute peaks in Fig. 13(b) and bun-like peaks in Fig. 13(c) that

represent the crystal and amorphous structures, respectively. This finding agrees with experimental

observations, which confirm the presence of graphitic crystal structures and amorphous stacking in

C black [29–33].

3.3 Temperature and Density-dependent C Condensation
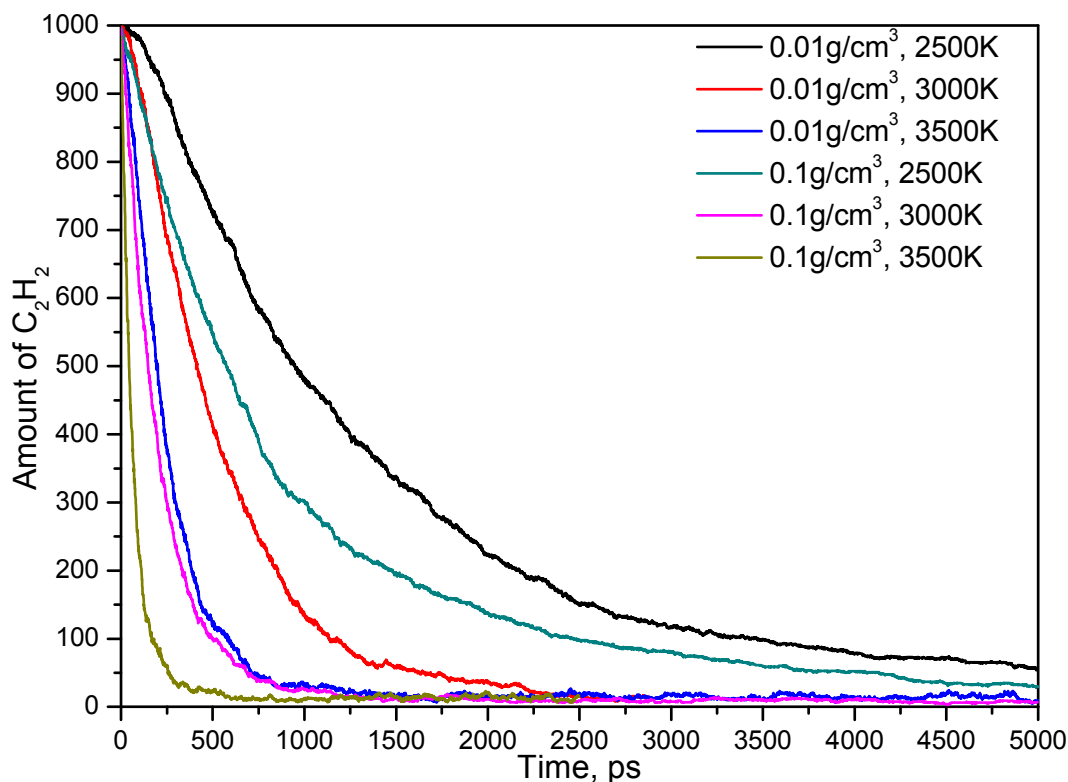
Fig. 14 C_2H_2 decay under different conditions.

As stated previously, within a simulation time of 5 ns, acetylene pyrolysis under different

densities and temperatures undergo similar evolution, but with a rate difference. In this section, we

focus on the influence of temperature and density on the evolution. From the above discussion, the

decay of C_2H_2 and the increase in the size of the maximal species can be indicative of this evolution.

In total, Fig. 14 exhibits that the higher temperature and the higher density lead to faster decay of

C_2H_2, and both temperature and density perform important functions in the decay. High temperature

weakens chemical bonds, whereas low density facilitates entropy increases. Both conditions aid

C_2H_2 dissociation, which is highly evident in the case of 0.01 g/cm^3 (the lowest density in the

simulations) and 3500 K (the highest temperature in the simulations). As demonstrated in Figs s5 and s6 of ESI, C species without H or with one H atom, i.e., C_4, C_4H, C_6, and C_6H, are dominant. When temperature decreases, H atoms on C species increase. For example, Figs s7 and s8 in ESI show the dominant populations of C_4H, C_4H_2, C_6H, and C_6H_2.
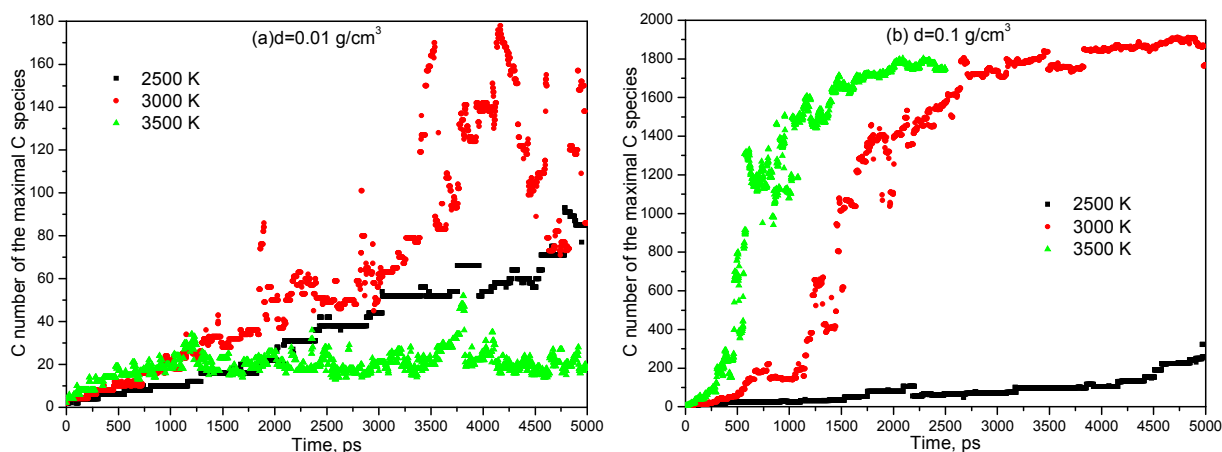
Fig. 15 Evolution of C numbers of the maximal C species at densities of (a) 0.01 and (b) 0.1 g/cm^3.

The size of the maximal C species varies widely from the above C_2H_2 decay. In the case of 0.01 g/cm^3 density, Fig. 15(a) represents the evolution of the largest C species proceed differently at the three temperatures within the simulation time range. These different evolutions can be explainable, as a higher temperature accelerates reactions but does not always accelerate C condensation. Before 1200 ps, the higher temperature leads to the more rapid size increase, because higher temperature causes faster H abstraction and more collision opportunities among C species, i.e., the faster C condensation. However, on the other hand, higher temperature can also accelerate the dissociation of condensed C species. Thus, a size balance occurs after 1200 ps at 3500 K. According to this result, we can find a gradual size increase at 2500 K and a rapid size increase to a top, and then a fluctuation at 3000 K. These tendencies can also be roughly found in the case of 0.1 g/cm^3 for the same reason (Fig. 5(b)). Given that species size is strongly dependent on species amount, these evolution characteristics under different conditions can be understood by amount evolution (see Fig. s9 of ESI).

From the above discussion, we can see that, within the time range of the simulations, C black formation is not a necessary result. This finding suggests that certain new structures, such as carbine, can be obtained under ideal selected conditions.

4. Conclusions

We imaged C black formation from acetylene pyrolysis at temperatures of 2500, 3000, and 3500 K. As a result, except from the evolution velocity, we find the formation is less dependent on the assigned acetylene density and temperature. The formation undergoes the following stages, namely, chain elongation, chain branching, cyclization and cycle condensation, and folding of condensed cycles. The simulated structures of C black are comparable to those of experimental observations. At the same time, the results validate the selected molecular reactive force field, Reax FF, in dealing with acetylene pyrolysis.

Several intermediate processes in simulations, such as further chain elongation, chain branching, chain fusion to cycles, and condensed cycles, are widely different from the reported observations at relatively low temperatures. These results suggest that the polyyne chains are stable at high temperature, and that acetylene pyrolysis to carbyne chains is possible if we can control the conditions perfectly.

Corresponding Author

Prof. Zhang Chaoyang, email: chaoyangzhang@caep.cn.

Electronic Supplementary Information

It contains comparison of pyrolysis evolution under various conditions; evolution of C11-C20 under

the condition of 0.1 g/cm^3 and 3500 K, C4, C6 particles under the condition of 0.01 g/cm^3 and total

amount of all C particles under different conditions.

References

(1) M. P. Anantram and F. Leonard, *Rep. Prog. Phys.*, 2006, **69**, 507-561.

(2) P. J. F. Harris, Carbon Nanotube Science: Synthesis, Properties and Application. Cambrige University Press, 2009.

(3) H. S. P. Wong and D. Akinwande, Carbon Nanotube and Graphene Device Physics. Cambrige University Press, 2011.

(4) D. R. Dreyer, S. Park, C.W. Bielawski and R. S. Ruoff, *Chem. Soc. Rev.*, 2010, **39**, 228-240.

(5) S. Stankovich, D. A. Dikin, G. H. B. Dommett, K. M. Kohlhaas, E. J. Zimney, E. A. Stach, R. D. Piner, S. T. Nguyen and R. S. Ruoff, *Nature*, 2006, **442**, 282-286.

(6) J. Zhang, X. Liu, R. Blume, A. Zhang, R. Schlögl and D. S. Su, *Science*, 2008, **322**, 73-77.

(7) L. Justin, M. Daniel, A. Richard, L. Frederick and A. Ilhan, *ACS Nano*, 2009, **3**, 3945-3954.

(8) A. Bagri, C. Mattevi, M. Acik, Y. J. Chabal, M. Chhowalla and V. B. Shenoy, *Nat. Chem.*, 2010, **2**, 581-587.

(9) S. Stankovich, *Carbon*, 2007, **45**, 1558-1565.

(10) L. Ravagnan, *Phys. Rev. Lett*. 2002, **89**, 285506.

(11) A. Capasso, E. Longhin, A. D'Anna, M. Camatini and M. Gualtieri, In Coarse, Fine and Ultrafine PM Impact on In Vitro Systems. Effects and Mechanisms of the Different Fractions; Environmental Health: Boston, MA, 2013.

(12) H. Bockhorn, A. D'Anna, A. F. Sarofim and H. Wang, Combustion Generated Fine Carbonaceous Particles; Karlsruhe University Press: Karlsruhe, Germany, 2009.

(13) M. Steinberg and H. Cheng, *Int. J. Hydrogen Energy*, 1989, **14**, 797-820.

(14) N. Z. Muradov, *Int. J. Hydrogen Energy*, 1993, **18**, 211-215.

(15) A. Strachan, A. C. T. van Duin, D. Chakraborty, S. Dasgupta and W. A. Goddard III, *Phys. Rev. Lett.*, 2003, **91**, 098301.

(16) K. I. Nomura, R. K. Kalia, A. Nakano, P. Vashishta, A. C. T. van Duin and W. A. Goddard III, *Phys. Rev. Lett.*, 2007, **99**, 148303.

(17) S. V. Zybin, W. A. Goddard III, P. Xu, A. C. T. van Duin and A. P. Thompson, *Appl. Phys. Lett.*, 2010, **96**, 081918.

(18) S. P. Han, A. C. T. van Duin, W. A. Goddard III and A. Strachan, *J. Phys. Chem. B*, 2011, **115**, 6534-6540.

(19) T. T. Zhou, S. V. Zybin, Y. Liu, F. L. Huang and W. A. Goddard III, *J. Appl. Phys.*, 2012, **111**, 124904.

(20) C. M. Fidel, M. K. Amar, F. R. Jr. Michael, A. C. T. van Duin and P. M. Jonathan, *Combust. Flame*, 2012, **159**, 1272-1285.

(21) C. M. Fidel and A. C. T. van Duin, *Combust. Flame*, 2013, **160**, 766-775.

(22) J. Ding, L. Zhang, Y. Zhang and K. Han, *J. Phys. Chem. A*, 2013,**117**, 3266-3278.

(23) C. Zhang, Y. Wen and X. Xue, *ACS Appli. Mater & Interface.*, 2014, **6**, 12235-12244.

(24) J. Ding, L. Zhang and K. Han, *Combust. Flame*, 2011, **158**, 2314-2324.

(25) M. Sansotera, C. L. Bianchi, G. Lecardi, G. Marchionni, P. Metrangolo, G. Resnati and Walter. Navarrini, *Chem. Mater*. 2009, **21**, 4498-4504.

(26) M. Wang, F. Xu, Q. Liu, H. Sun, R. Cheng, H. He, E. Stach and J. Xie, *Carbon*, 2011, **49**, 256-265.

(27) Y. Bin, C.Xu, D. Zhu and M. Matsuo, *Carbon*, 2002, **40**, 195-199.

(28) S. Lee, M. Kim, J. Kwak, G. Han, J. Park, T. Lee and K. Yoon, *Carbon*, 2010, **48**, 2030-2036.

(29) W. M. Hess and C. R. Hurd, in *Carbon Black,* edited by J-B. Donnet, R. C. Bansal and M-J. Wang. New York, 1993, pp. 91-106; and references therein.

(30) J. I. Paredes, M. Gracia, A. Martinez-Alnoso and J. M. D. Tascon, *J. Colloid Interface Sci.*, 2005, **288**, 190-199.

(31) W. Niedermeier, J. Stierstorfer, S. Kreitmerer, O. Metz and D. Goritz, Morphological Investigations on Carbon Black Particles by Atomic Force Microscopy. Rubber Chemistry and Technology, published by ACS, 1994, **67**, 148-158.

(32) W. Xu, T. W. Zerda, H. Raab and D. Goritz, *Carbon*, 1997, **35**, 471-474

(33) M. Frenklach, *Phys. Chem. Chem. Phys.* 2002, **4**, 2028-2037.

(34) G. B. Skinner and E. M. Sokoloski, *J. Phys. Chem.* 1960, **64**, 1952-1953.

(35) C. Aten and E. Greene, *Combust. Flame* 1961, **5**, 55-64.

(36) J. Kiefer, S. Kapsalis, M. Al-Alami and K. Budach, *Combust. Flame*, 1983, **51**, 79-93.

(37) M. Frenklach, S. Taki, M. Durgaprasad and R. Matula, *Combust. Flame,* 1983, **54**, 81-101.

(38) X. Xu and P. Pacey, *Phys. Chem. Chem. Phys.* 2005, **7**, 326-333.

(39) B. Shukla and M. Koshi, *Anal. Chem.* 2012, **84**, 5007-5016.

(40) K. Norinaga, O. Deutschmann and K. J. Huttinger, *Carbon,* 2006, **44**, 1790-1800.

(41) K. Norinaga, V. M. Janardhanan and O. Deutschmann, *Int. J. Chem. Kinet.* 2008, **40**, 199-208.

(42) N. E. Sanchez, A. Callejas, A. Millera, R. Bilbao and M. U. Alzueta, *Chem. Eng. Trans.* 2010, **22**, 131-136.

(43) N. E. Sanchez, A. Callejas, A. Millera, R. Bilbao and M. U. Alzueta, *Energy*, 2012, **43**, 30-36.

(44) N. E. Sanchez, A. Millera, R. Bilbao and M. U. Alzueta, *Anal. Appl. Pyrolysis* 2013, **103**, 126-133.

(45) C. Wu, H. Singh and R. Kern, *Int. J. Chem. Kinet.*, 1987, **19**, 975-996.

(46) Y. Hidaka, K. Hattori, T. Okuno, K. Inami, T. Abe and T. Koike, *Combust. Flame*, 1996, **107**, 401-417.

(47) S. J. Plimpton, *J. Comput. Phys.*, 1995, **117**, 1-19.

(48) H. M. Aktulga, J. C. Fogarty, S. A. Pandit and A. Y. Grama, *Parallel Comput.*, 2012, **38**, 245-259.

(49) W. Hoover, *Phys. Rev. A*, 1985, **31**, 1695-1697.

(50) A.C.T. Van Duin, S. Dasgupta, F. Lorant and W. A. Goddard Ⅲ, *J. Phys. Chem. A*, 2001, **105**, 9396−9409.

(51) D. W. Brenner, *Phys. Rev. B.* 1990, **42**, 9458-71.

(52) D. W. Brenner, O. A. Shenderova, J. Harrison, S. J. Stuart, B. Ni and S. B. Sinnott, *J Phys: Condensed Matter.* 2002, **14**, 783-802.

(53) K. Chenoweth, A. C. T. Van Duin and W. A. Goddard Ⅲ, *J. Phys. Chem. A* 2008, **112***, 1040-1053.

(54) A. J. Page and B. Moghtaderi, *J. Phys. Chem. A* 2009, **113***, 1539-1547.

(55) X. Cheng, Q. Wang, J. Li, J. Wang and X. Li, *J. Phys. Chem. A* 2012, **116**, 9811-9818.

(56) Q. Wang, X. Hua, X. Cheng, J. Li and X. Li, *J. Phys. Chem. A* 2012, **116**, 3794-3801.

(57) Q. Wang, J. Wang, J. Li, N. Tan and X. Li, *Combust. Flame*, 2011, **158**, 217-216.

(58) N. Lümmen, *Phys. Chem. Chem. Phys.*, 2010, **12**, 7883-7893.

(59) H. Zhang, G. Li, F. Wang and Y. Liang, *Commun. Comput. Chem.*, 2014, **2**, 1-8.

(60) Y. Luo, Handbook of Bond Dissociation Energies. Beijing, Science Press, 2005.

(61) Y. Wang, A. J. Page, Y. Nishimoto, H. J. Qian, K. Morokuma and S. Irle, *J. Am. Chem. Soc.* 2011, **133**,

18837-18842.

(62) A. G. Whittaker, *Science*, 1978, **200**, 763-764.

(63) M. Liu, V. Artyukhov, H. Lee, F. Xu and B. Yakobson, *ACS Nano*, 2013, **7**, 10075-10082.

(64) W. A. Chalifoux and R. R. Tykwinski, *Nat. Chem.*, 2010, **2**, 967-971.

(65) M. P. Allen and D. J.Tildesley, *Computer Simulation of Liquids*, Clarendon Press, Oxford Science Publications, 1987.

(66) R. K. McMullan, A. Kvick and P. Popelier, *Acta Crystallogr., Section B*, 1992, **48**, 726-731.

(67) G. J. H. van Nes and A. Vos, *Acta Crystallogr., Section B*, 1979, **35**, 2580-2593.